JCI The Journal of Clinical Investigation

CCL17-expressing dendritic cells drive atherosclerosis by restraining regulatory T cell homeostasis in mice

Christian Weber, … , Tobias Junt, Alma Zernecke

J Clin Invest. 2011;121(7):2898-2910. https://doi.org/10.1172/JCI44925.

Research Article **Cardiology**

Immune mechanisms are known to control the pathogenesis of atherosclerosis. However, the exact role of DCs, which are essential for priming of immune responses, remains elusive. We have shown here that the DC-derived chemokine CCL17 is present in advanced human and mouse atherosclerosis and that $CCL17^+$ DCs accumulate in atherosclerotic lesions. In atherosclerosis-prone mice, *Ccl17* deficiency entailed a reduction of atherosclerosis, which was dependent on Tregs. Expression of CCL17 by DCs limited the expansion of Tregs by restricting their maintenance and precipitated atherosclerosis in a mechanism conferred by T cells. Conversely, a blocking antibody specific for CCL17 expanded Tregs and reduced atheroprogression. Our data identify DC-derived CCL17 as a central regulator of Treg homeostasis, implicate DCs and their effector functions in atherogenesis, and suggest that CCL17 might be a target for vascular therapy.

CCL17-expressing dendritic cells drive atherosclerosis by restraining regulatory T cell homeostasis in mice

Christian Weber,[1,2,3] Svenja Meiler,[3,4] Yvonne Döring,[1,5] Miriam Koch,[4] Maik Drechsler,[3,4] Remco T.A. Megens,[1,3,6] Zuzanna Rowinska,[3,7] Kiril Bidzhekov,[1,3] Caroline Fecher,[4] Eliana Ribechini,[8] Marc A.M.J. van Zandvoort,[2,3] Christoph J. Binder,[9] Ivett Jelinek,[5] Mihail Hristov,[1,3] Louis Boon,[10] Steffen Jung,[11] Thomas Korn,[12] Manfred B. Lutz,[8] Irmgard Förster,[13] Martin Zenke,[5] Thomas Hieronymus,[5] Tobias Junt,[14] and Alma Zernecke[2,4]

[1]Institute for Cardiovascular Prevention, Ludwig-Maximilians-Universität München, Munich, Germany. [2]Cardiovascular Research Institute Maastricht (CARIM), Maastricht University, Maastricht, The Netherlands. [3]Institute for Molecular Cardiovascular Research (IMCAR), Medical Faculty, RWTH Aachen University, Aachen, Germany. [4]Rudolf Virchow-Zentrum/DFG–Research Center for Experimental Medicine, University of Würzburg, Würzburg, Germany. [5]Institute for Biomedical Engineering, Department of Cell Biology, [6]Interdisciplinary Centre for Clinical Research, and [7]European Vascular Center Aachen-Maastricht, University Hospital, RWTH Aachen University, Aachen, Germany. [8]Institute of Virology and Immunobiology, University of Würzburg, Würzburg, Germany. [9]Center for Molecular Medicine (CeMM) of the Austrian Academy of Sciences and Department of Laboratory Medicine, Medical University of Vienna, Vienna, Austria. [10]Bioceros BV, Utrecht, The Netherlands. [11]Department of Immunology, Weizmann Institute of Science, Rehovot, Israel. [12]Department of Neurology, Klinikum rechts der Isar, Technical University Munich, Munich, Germany. [13]Molecular Immunology, IUF–Leibniz Research Institute for Environmental Medicine, Düsseldorf, Germany. [14]Novartis Pharma AG, Basel, Switzerland.

Immune mechanisms are known to control the pathogenesis of atherosclerosis. However, the exact role of DCs, which are essential for priming of immune responses, remains elusive. We have shown here that the DC-derived chemokine CCL17 is present in advanced human and mouse atherosclerosis and that CCL17$^+$ DCs accumulate in atherosclerotic lesions. In atherosclerosis-prone mice, *Ccl17* deficiency entailed a reduction of atherosclerosis, which was dependent on Tregs. Expression of CCL17 by DCs limited the expansion of Tregs by restricting their maintenance and precipitated atherosclerosis in a mechanism conferred by T cells. Conversely, a blocking antibody specific for CCL17 expanded Tregs and reduced atheroprogression. Our data identify DC-derived CCL17 as a central regulator of Treg homeostasis, implicate DCs and their effector functions in atherogenesis, and suggest that CCL17 might be a target for vascular therapy.

Introduction

Atherosclerosis is a chronic inflammatory disease of the arterial wall, modulated by immune responses (1). Besides monocytes/macrophages, other mononuclear cells, namely T cells and DCs, can be detected within atherosclerotic lesions (2). DCs are professional antigen-presenting cells that can be divided into several subtypes and are essential for priming of immune responses (3, 4). A network of DCs has been identified in the arterial intima of healthy young individuals (5), and an accumulation of DCs can be observed in the intima and adventitia of atherosclerosis-susceptible regions in mice (6, 7). In advanced human plaques, increased numbers of DCs are found in clusters with T cells (8, 9). Moreover, DC-derived chemokines, such as CCL17 (also known as thymus- and activation-regulated chemokine [TARC]) and CCL22, are present in atherosclerotic lesions (10).

Modified lipoproteins, e.g., oxidized low-density lipoprotein (oxLDL), deposited in the arterial wall are taken up by DCs to initiate early lesion formation (11) and may instigate an early immune activation of vascular DCs. Accordingly, oxLDL induces the upregulation of costimulatory molecules on DCs and increases T cell proliferation (12), with lipid-loaded DCs remaining capable of priming CD4$^+$ T cells in atherosclerosis (13). Consequently, antigen-specific and clonally expanded T cells were found in early plaques of patients (2, 14). Different T cell subpopulations with a specific signature of pro- or antiinflammatory cytokines control the atherogenic process (15–20). In particular, Tregs, which suppress activation of the immune system, have been characterized as powerful inhibitors of atherosclerosis (18, 21). However, cell types important in restricting Treg responses have not been identified.

Despite evidence suggesting a role for DCs in the pathogenesis of atherosclerosis, the precise functions of DCs and their effector cytokines remain to be elucidated. Attempts at depleting this cell population for longer time periods have proven difficult. Following transient depletion of DCs in mice carrying a transgene encoding a diphtheria toxin receptor under the control of the CD11c promoter, proinflammatory effects of apoptotic CD11c$^+$ plaque macrophages (22) or prevailing effects of other cell subsets (A. Zernecke et al., unpublished observations) were observed, and mice lacking conventional DCs because of constitutive cell-specific expression of a suicide gene develop a myeloproliferative disorder (23). In an alternative approach, systemic immunization with oxLDL-loaded DCs has been explored for treatment of diet-induced atherosclerosis but has failed to yield effects on lesion development in the aortic root (24).

The DC chemokines CCL17 and CCL22 activate the chemokine receptor CCR4 and were first thought to preferentially promote T cell responses with a Th2 bias; however, emerging evidence sup-

Authorship note: Christian Weber, Svenja Meiler, and Yvonne Döring contributed equally to this work.

Conflict of interest: Tobias Junt is an employee of Novartis Pharma AG.

Citation for this article: *J Clin Invest.* 2011;121(7):2898–2910. doi:10.1172/JCI44925.

ports the notion that CCL17 can attract effector/memory T cells of the Th1 subtype but also Tregs (25–27). Although it is present in atherosclerotic lesions (10), the role of CCL17 in atherosclerosis has not been previously studied. As CCL17 is exclusively expressed by a myeloid-related mature subset of DCs (28), employing mice with a targeted replacement of the *Ccl17* gene by the enhanced green fluorescent protein gene (*Egfp*; $Ccl17^{E/E}$ mice) offers insights into the localization and function of this subset during atherosclerosis. Here we provide the first evidence to our knowledge that $CCL17^+$ DCs restrain the homeostasis of Tregs and thereby promote atherosclerosis.

Results

$CCL17^+$ DCs accumulate in atherosclerotic lesions. $CCL17^+$ DCs are detectable not only in LNs (Supplemental Figure 1; supplemental material available online with this article; doi:10.1172/JCI44925DS1) but also in various other organs (28). We tested whether $CCL17^+$ DCs are part of a resident intimal DC network that can accumulate at arterial sites predisposed to atherosclerosis and initiate nascent lesion formation (5, 11). Healthy CD11c-EYFP reporter mice were analyzed by immunofluorescence and multiphoton microscopy to identify cells expressing the widely used DC marker CD11c. We frequently detected $EYFP^+$ cells positive for MHC-II in the intima and adventitia of the aorta and aortic root and in cardiac valves (Figure 1A and Supplemental Videos 1 and 2). In contrast, healthy control $Ccl17^{E/+}$ and $Ccl17^{E/E}$ apolipoprotein E–deficient ($Apoe^{-/-}$) mice displayed negligible $EGFP^+CD11c^+$ DC content at baseline, as revealed by flow cytometry of aortic cell suspensions, whereas frequencies of $EGFP^+CD11c^+$ DCs were increased in aortic segments of $Ccl17^{E/+}Apoe^{-/-}$ and $Ccl17^{E/E}Apoe^{-/-}$ mice fed a high-fat diet, with no difference between genotypes (Figure 1B, 78.6 ± 16.4 and 77.5 ± 11.7 $EGFP^+CD11c^+$ DCs, respectively). This was also evident by microscopic analysis tracing $EGFP^+$ DCs to subluminal and core regions of aortic root plaques in $Ccl17^{E/+}Apoe^{-/-}$ and $Ccl17^{E/E}Apoe^{-/-}$ mice with diet-induced and spontaneous atherosclerosis (Figure 1, C–E, and Supplemental Video 3).

Analysis of peripheral LNs and bone marrow–derived DCs (BMDCs) from $Ccl17^{E/+}$, $Ccl17^{E/E}$, $Ccl17^{E/+}Apoe^{-/-}$, and $Ccl17^{E/E}Apoe^{-/-}$ mice (Supplemental Results) confirmed that CCL17 expression is restricted to a phenotypically mature subset of $CD11c^+CD11b^+CD8\alpha^-CD115^-F4/80^-440c^-PDCA\text{-}1^-$ DCs, which display increased expression of MHC-II (28) and costimulatory molecules (CD40, CD80, CD86) and are distinct from monocyte-derived TNF/iNOS-producing (Tip) DCs (29). To assess the phenotype of lesional DCs, we analyzed aortic cell suspensions by flow cytometry. Despite the low abundance of these cells, our data revealed that $EGFP^+CD11b^+CD11c^+$ aortic DCs within lesions, as in LNs, express increased levels of MHC-II and costimulatory molecules, as compared with $EGFP^-CD11b^+CD11c^+$ DCs, with no differences between $Ccl17^{E/+}Apoe^{-/-}$ and $Ccl17^{E/E}Apoe^{-/-}$ mice (Supplemental Figure 2A and data not shown), confirming a distinct mature phenotype in lesional DCs (28).

The mRNA expression of *Ccl17* was elevated in $Apoe^{-/-}$ mice with advanced lesions (3.8 ± 0.8–fold vs. healthy aortas, $n = 4$, $P < 0.01$) but also in human carotid endarterectomy specimens (13.7 ± 3.5–fold vs. macroscopically healthy arteries, $n = 3$, $P < 0.005$), in line with the presence of CCL17 in human atherosclerosis (10). Whereas DCs in large arteries thus do not express CCL17 under steady-state conditions, our data clearly indicate that $CCL17^+CD11c^+$ DCs accumulate in atherosclerotic arteries. Notably, $EGFP^+CCL17^+$ DCs were detectable in advanced aortic root plaques and adventitia of $Apoe^{-/-}$ mice reconstituted with $Ccl17^{E/+}Apoe^{-/-}$ BM (Supplemental Figure 2B), suggesting that these cells are directly recruited from the BM during lesion progression or emerge from BM-derived and matured resident DCs.

In general, DCs migrate to draining LNs to initiate and modulate immune responses (3, 4). Here we show that vascular DCs harbor the capacity to migrate to lymphatic tissue. After footpad injection into $Apoe^{-/-}$ mice, $CD11c^+$ DCs isolated from naive CD11c-EYFP aortas accumulated in popliteal LNs after 18 hours (Supplemental Figure 3A). Moreover, both $EGFP^+$ $Ccl17^{E/+}$ BMDCs and $Ccl17^{E/E}$ BMDCs migrated to popliteal LNs after footpad injection (Supplemental Figure 3B). To more directly evaluate a possible exit of DCs from the aorta, we performed a model of orthotopic aortic transplantation. Notably, $CD11c^+EGFP^+$ DCs were detected in para-aortic LNs of $Apoe^{-/-}$ mice that underwent transplantation with $Ccl17^{E/+}Apoe^{-/-}$ or $Ccl17^{E/E}Apoe^{-/-}$ aortas (but not with $Ccl17^{+/+}Apoe^{-/-}$ aortas), and were found to highly express CD45, MHC-II and CD11b (Supplemental Figure 3C). These data support the concept that aortic $CCL17^+$ DCs may have the potential to travel to regional LNs to exert systemic effects.

Deficiency of Ccl17 reduces atherosclerosis in $Apoe^{-/-}$ mice. We next studied the role of $CCL17^+$ DCs in atherosclerotic lesion formation. Compared with that in $Ccl17^{+/+}Apoe^{-/-}$ controls, plaque formation in the aortic root and the aorta was significantly reduced in $Ccl17^{E/E}Apoe^{-/-}$ mice after 6 months of normal chow (Figure 2A). This was associated with a decrease in the relative content of aortic macrophages (Figure 2B) and an increase in SMCs (9.0% ± 2.0% vs. 1.9% ± 0.6% $smoothelin^+$ plaque area, $P < 0.005$), implying a more stable plaque phenotype in $Ccl17^{E/E}Apoe^{-/-}$ mice. Lesion formation was also reduced in the aortic root and aorta of $Ccl17^{E/E}$ versus $Ccl17^{+/+}Apoe^{-/-}$ mice after 12 weeks of high-fat diet (Supplemental Figure 4A). In contrast, lesion formation did not differ between $Ccl17^{+/+}Apoe^{-/-}$ and $Ccl17^{E/E}Apoe^{-/-}$ mice reconstituted with $Ccl17^{+/+}Apoe^{-/-}$ BM, indicating that $CCL17^+$ effector cells predominantly originate from BM (Supplemental Figure 4B). We also evaluated the role of the CCL17 receptor CCR4 in BM-derived cells. As compared with mice transplanted with $Ccr4^{+/+}$ BM, $Ldlr^{-/-}$ mice reconstituted with $Ccr4^{-/-}$ BM and fed a high-fat diet did not display alterations in atherosclerotic plaque size or composition (Supplemental Figure 4C and data not shown). To assess the contribution of CCL17 to lesion progression, we reconstituted $Apoe^{-/-}$ mice bearing established atherosclerotic lesions after 12 weeks of high-fat diet with $Ccl17^{+/+}Apoe^{-/-}$ or $Ccl17^{E/E}Apoe^{-/-}$ BM. After an additional 12 weeks of high-fat diet, lesion progression in the aortic root and the aorta was significantly delayed in recipients of $Ccl17^{E/E}Apoe^{-/-}$ BM versus those receiving $Ccl17^{+/+}Apoe^{-/-}$ BM (Supplemental Figure 4D).

CCL17 recruits T cells to sites of atherogenesis and inflammation. Numbers of $CD3^+$ T cells were markedly reduced in atherosclerotic lesions of $Ccl17^{E/E}Apoe^{-/-}$ versus $Ccl17^{+/+}Apoe^{-/-}$ mice (Figure 2C). To evaluate whether lesional $CCL17^+$ DCs function to recruit $CD4^+$ T cells and/or Tregs to the atherosclerotic aorta, we performed adoptive transfer studies. Equal numbers of labeled $CD4^+$ T cells and Tregs were transferred side-by-side into atherosclerotic $Ccl17^{+/+}Apoe^{-/-}$ or $Ccl17^{E/E}Apoe^{-/-}$ mice. Indeed, frequencies of $CD4^+$ T cells accumulating in the aorta of $Ccl17^{E/E}Apoe^{-/-}$ mice after 3 days were reduced, as compared with $Ccl17^{+/+}Apoe^{-/-}$ aortas or non-injected controls, whereas Treg recruitment was less pronounced and unaltered in $Ccl17^{E/E}Apoe^{-/-}$ mice (Figure 3A). To confirm that DC-derived CCL17 attracts T cells, we used Transwell chemotaxis

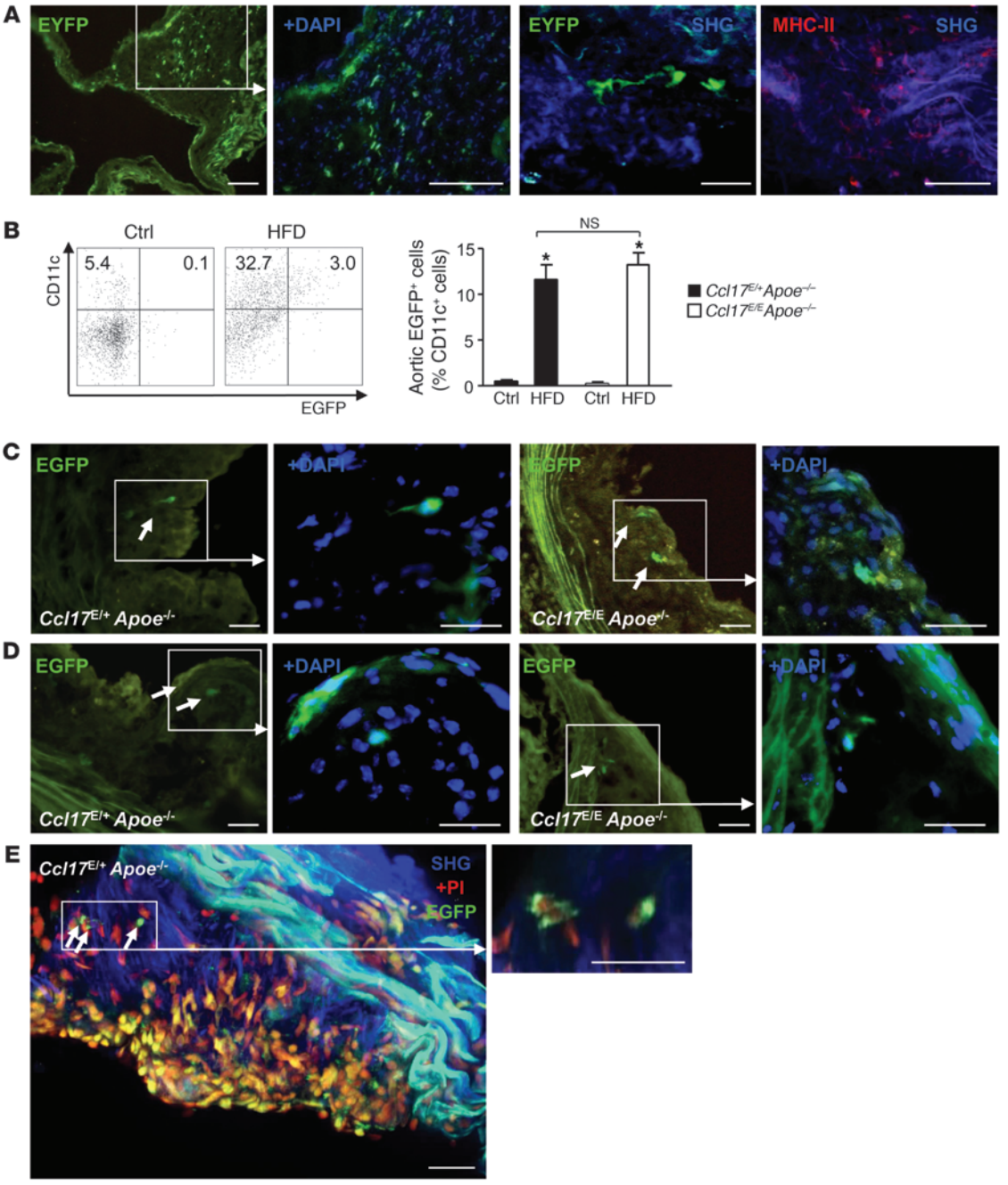

Figure 1

CCL17-expressing DCs accumulate within atherosclerotic lesions. (**A**) A network of EYFP$^+$CD11c$^+$ DCs (green) can be detected by immunofluorescence in the aortic root (left 2 panels, scale bars: 50 μm) and by multiphoton microscopy in the en face prepared aorta (middle right panel, scale bar: 20 μm) of CD11c-EYFP reporter mice; representative maximum intensity projection of a 30-μm-thick volume is shown. Multiphoton microscopy of an en face prepared aorta of a wild-type mouse stained for MHC-II$^+$ (red); collagen was visualized by SHG (blue, far right panel, scale bar: 20 μm). (**B**) Quantification of EGFP$^+$CD11c$^+$ DCs in aortas of healthy *Ccl17*$^{E/+}$*Apoe*$^{-/-}$ and *Ccl17*$^{E/E}$*Apoe*$^{-/-}$ mice or after high-fat diet (HFD) feeding using enzymatic digestion and FACS analysis; representative dot blots and percentages within quadrants are shown ($n = 6$ each). *$P < 0.05$. ctrl, control. (**C** and **D**) EGFP$^+$ DCs (green, indicated by arrows) in the aortic root of *Ccl17*$^{E/+}$*Apoe*$^{-/-}$ and *Ccl17*$^{E/E}$*Apoe*$^{-/-}$ mice after 12 weeks of high-fat diet feeding (**C**) and after 6 months of normal chow (**D**); cell nuclei are counterstained by DAPI (blue); scale bars, 50 μm. (**E**) Maximum intensity projection of a *z*-stack (left) and high-magnification *z*-slice (right) with EGFP$^+$ DCs (bright green cytoplasmic staining; arrows) in the atherosclerotic aortic root of a *Ccl17*$^{E/+}$*Apoe*$^{-/-}$ mouse on normal chow. Nuclei are counterstained with PI (red); PI staining can also appear yellow due to background fluorescence. Collagen is visible due to SHG (blue). Scale bars: 40 μm.

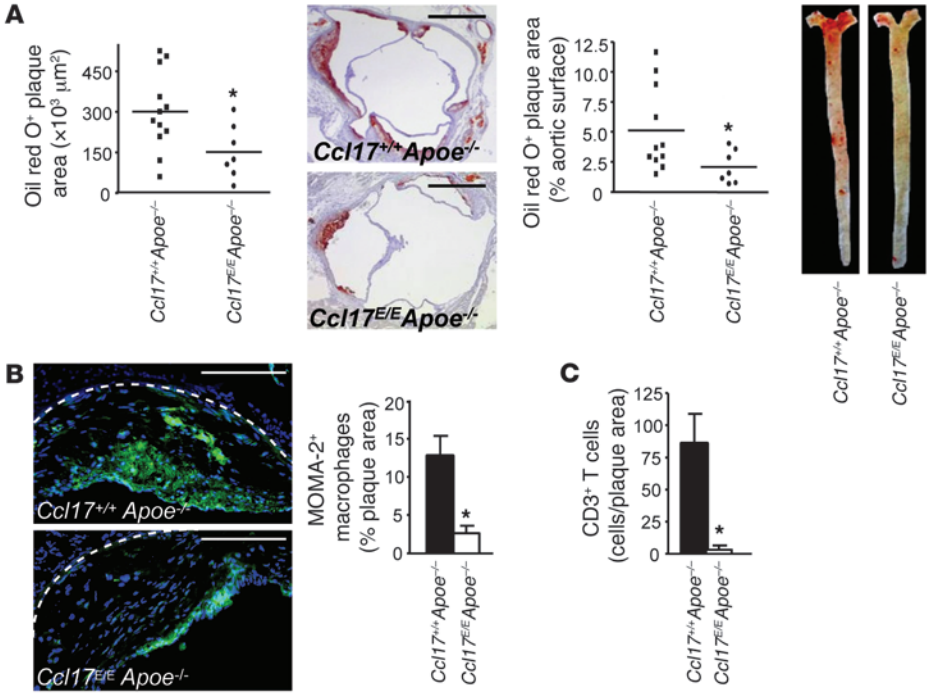

Figure 2

Ccl17 deficiency reduces atherosclerosis. (**A**) Atherosclerotic lesions were quantified in the aortic root and thoracoabdominal aorta after staining with oil red O in *Ccl17*$^{+/+}$*Apoe*$^{-/-}$ and *Ccl17*$^{E/E}$ *Apoe*$^{-/-}$ mice on normal chow for 6 months; individual data points represent average plaque area per mouse; horizontal bars denote mean. Representative images of the aortic root (scale bars: 500 μm) and the thoracoabdominal aorta are shown. (**B** and **C**) The relative content of MOMA-2$^+$ macrophages (scale bars: 200 μm) and CD3$^+$ T cells (**C**) per plaque area was analyzed by quantitative immunofluorescence. Representative images of macrophage staining (green) are shown (**B**); cell nuclei are counterstained by DAPI (blue); dashed lines indicate the internal elastic lamina. *$P < 0.05$.

assays, where *Ccl17*$^{+/+}$ BMDCs in the lower chamber induced significantly more CD4$^+$ T cell migration than *Ccl17*$^{E/E}$ BMDCs (Figure 3B). In an air pouch model, recombinant mouse CCL17 dose- and time-dependently enhanced the inflammatory recruitment of CD4$^+$ T cells and Tregs in vivo, compared with PBS-injected controls (Figure 3C and Supplemental Results). In contrast to sites of inflammation, homing of adoptively transferred CD3$^+$CD4$^+$ T cells and Tregs to peripheral LNs was not impaired in *Ccl17*$^{E/E}$ mice after 2 hours (Supplemental Figure 5), implying a redundant role of CCL17 in T cell homing to LNs. Our data indicate that CCL17 is involved in recruiting CD4$^+$ T cells to sites of inflammation, whereas their recruitment to LNs can occur independently of CCL17.

Expansion of Tregs in the absence of CCL17. Analyzing the distribution of T cells in LNs, we found higher frequencies of CD4$^+$ T cells and an expansion of CD4$^+$CD25$^+$Foxp3$^+$ Tregs in *Ccl17*$^{E/E}$ versus *Ccl17*$^{+/+}$ mice (Figure 3, D and E) and in *Ccl17*$^{+/+}$*Apoe*$^{-/-}$ versus *Ccl17*$^{E/E}$*Apoe*$^{-/-}$ mice (Supplemental Figure 6A). This was associated with concordant alterations in both quiescent CD62L$^+$ and activated CD44$^+$CD4$^+$CD25$^+$ Tregs (ref. 29 and data not shown), increased *Foxp3* mRNA expression within LNs (Figure 3F and Supplemental Figure 6B), and elevated IL-10 but reduced IFN-γ serum levels (Supplemental Figure 6C). Serum levels of total IgG antibodies to malondialdehyde-modified LDL were reduced, with higher IgG_1 but lower IgG_{2c} titers in *Ccl17*$^{E/E}$ versus *Ccl17*$^{+/+}$*Apoe*$^{-/-}$ mice (Supplemental Figure 6D), indicating impaired immune priming and T cell help for antibody production.

To evaluate the number of Tregs within lesions, we analyzed *Ldlr*$^{-/-}$ mice reconstituted with *Foxp3gfp.KI* BM at different time points of lesion formation. Whereas numerous Foxp3$^+$ (GFP$^+$) cells could be found in LNs of *Ldlr*$^{-/-}$ mice reconstituted with *Foxp3gfp.KI* BM (Supplemental Figure 7), only a few isolated Foxp3$^+$ cells were detectable in the adventitia of mice before diet and during atheroprogression, and in atherosclerotic lesions in the aortic root after 5 and 9 weeks of high-fat diet (Figure 3G and Supplemental Figure 7). Accordingly, real-time PCR analysis of atherosclerotic aortas (which may also include adventitial Tregs) revealed increased *Foxp3* mRNA expression in the aorta of *Ccl17*$^{E/E}$*Apoe*$^{-/-}$ as compared with *Ccl17*$^{+/+}$*Apoe*$^{-/-}$ mice (Figure 3H). To substantiate these data, we performed flow cytometric analysis of aortic cell suspensions, which revealed a significant increase in the low aortic content of Tregs in *Ccl17*$^{E/E}$*Apoe*$^{-/-}$ versus *Ccl17*$^{+/+}$*Apoe*$^{-/-}$ mice (Figure 3I). Together with the marginal recruitment of Tregs to the inflamed aorta, these data imply that CCL17$^+$ DCs are involved in homeostatic mechanisms beyond the attraction of Tregs at sites of inflammation and lymphoid tissue.

CCL17$^+$ DCs control Treg maintenance. To assess mechanisms of Treg expansion, we studied whether CCL17 affects the polarization of naive T cells toward Tregs. In T cell polarization assays using TGF-β in vitro, addition of CCL17 did not alter the frequencies of Foxp3$^+$ Tregs among CD4$^+$ T cells (Supplemental Figure 8). However, when monitoring the fate of injected CFSE$^+$CD4$^+$CD25$^-$ T cells in vivo, we observed an expansion of CFSE$^+$Foxp3$^+$ Tregs or an increased rate of conversion, as evident by significantly higher frequencies of CFSE$^+$Foxp3$^+$ Tregs among CFSE$^+$ T cells, in *Ccl17*$^{E/E}$ mice as compared with *Ccl17*$^{+/+}$ mice (Figure 4A). Moreover, the proliferation of both CFSE$^+$Foxp3$^+$ Tregs and CFSE$^+$CD4$^+$ T cells was enhanced in *Ccl17*$^{E/E}$ versus *Ccl17*$^{+/+}$ mice (61.8% ± 7.3% vs. 42.4% ± 3.7% and 29.8% ± 5.6% vs. 8.5% ± 0.8%, respectively, $P < 0.05$, $n = 10$).

To address principal functions of CCL17$^+$ DCs in antigen-dependent interactions with T cells, we used OVA as an artificial antigen. Antigen-specific proliferation of CFSE-labeled OVA-specific OT-II CD4$^+$ T cells exposed to OVA-2–pulsed EGFP$^+$*Ccl17*$^{E/E}$ BMDCs or DCs sorted from peripheral LNs in vivo increased, when compared with EGFP$^+$*Ccl17*$^{E/+}$ DCs (Supplemental Results). To distinguish the underlying mechanisms, CD4$^+$ T cells or polarized Tregs were cocultured with DCs to engage in antigen-specific interactions in vitro. Indeed, OVA-2–pulsed EGFP$^+$*Ccl17*$^{E/E}$ BMDCs induced a more marked antigen-specific proliferation of OT-II CD4$^+$ T cells than

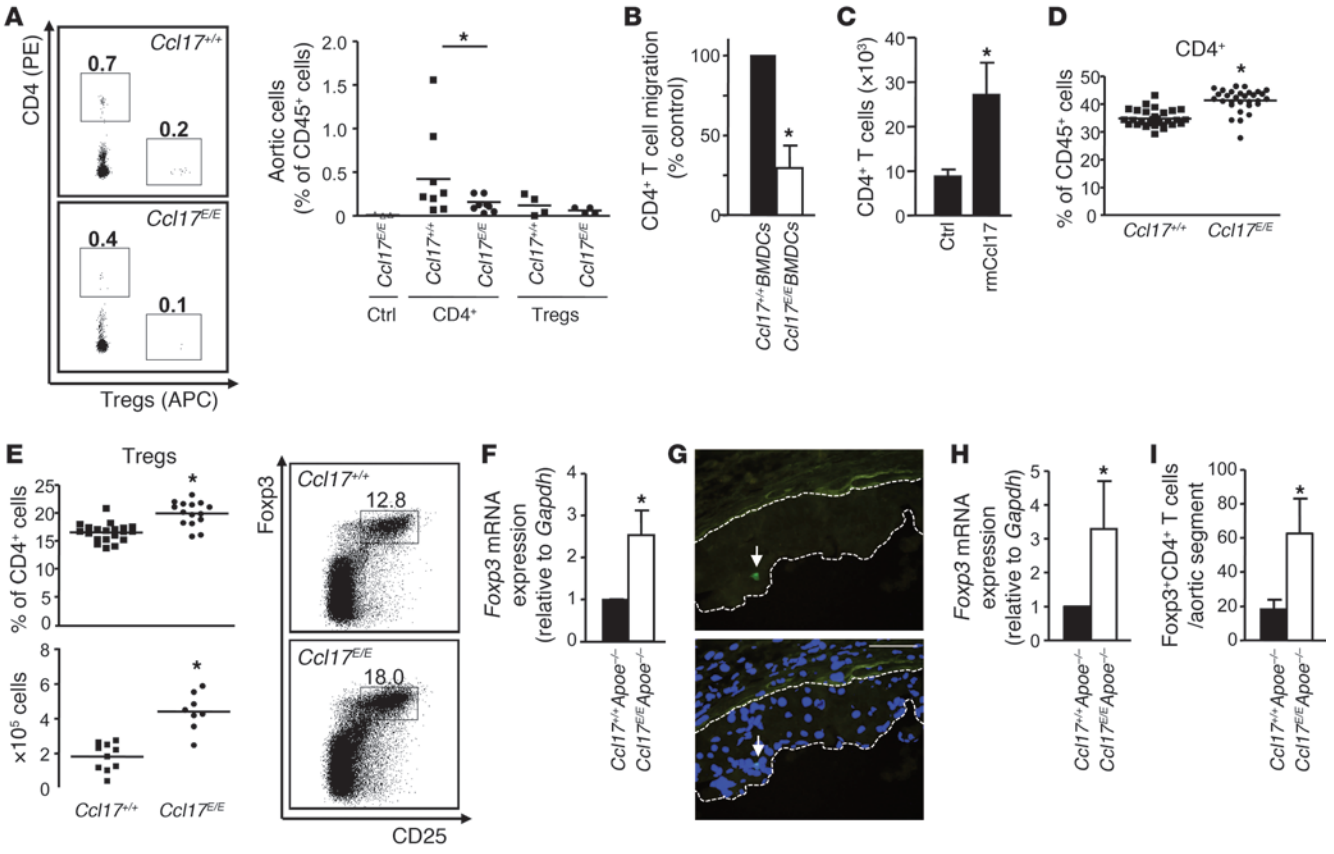

Figure 3

Ccl17 deficiency affects T cell distributions. (**A**) Quantification of PE-CD4+ T cells and APC-Tregs accumulating in atherosclerotic aortas of high-fat diet–fed *Ccl17*$^{+/+}$*Apoe*$^{-/-}$ and *Ccl17*$^{E/E}$*Apoe*$^{-/-}$ mice 3 days after adoptive transfer, using enzymatic digestion and FACS analysis. Representative dot plots depict frequencies of labeled cells among CD45+ aortic cells. Data points represent frequencies of transferred aortic cells in individual mice; horizontal bars denote mean of all mice. (**B**) Transwell migration of CD4+ T cells toward *Ccl17*$^{E/+}$ or *Ccl17*$^{E/E}$ BMDCs was quantified by FACS analysis ($n = 5$). (**C**) Absolute numbers of CD4+ T cells recruited to air pouches injected with PBS (ctrl, $n = 8$) or recombinant mouse CCL17 (50 ng/ml, $n = 9$) were quantified in lavage fluid after 4 hours. (**D** and **E**) Flow cytometric analysis of CD3+CD4+ T cells (**D**) and CD4+Foxp3+CD25+ Tregs (**E**) in LNs of *Ccl17*$^{+/+}$ and *Ccl17*$^{E/E}$ mice employing indicated surface markers. Representative dot plots as well as relative and absolute numbers of Tregs are shown; numbers in dot plots are percentage of CD4+ events. Data points represent frequencies of cells in individual mice; horizontal bars, mean of all mice. (**F**) *Foxp3* mRNA expression in LNs of *Ccl17*$^{+/+}$*Apoe*$^{-/-}$ and *Ccl17*$^{E/E}$*Apoe*$^{-/-}$ mice fed a high-fat diet ($n = 3$ each). (**G**) Detection of Foxp3+GFP+ cells (arrows, both panels) in atherosclerotic plaques of *Ldlr*$^{-/-}$ mice reconstituted with *Foxp3gfp.KI* BM after 9 weeks of high-fat diet; cell nuclei were counterstained by DAPI (blue, lower panel); dotted lines demarcate lesional area. Scale bars: 50 μm. (**H**) *Foxp3* mRNA expression in atherosclerotic aortas of *Ccl17*$^{+/+}$*Apoe*$^{-/-}$ and *Ccl17*$^{E/E}$*Apoe*$^{-/-}$ mice on high-fat diet ($n = 3$ each). (**I**) Quantification of CD4+CD25+Foxp3+ Tregs in atherosclerotic aortic segments of *Ccl17*$^{+/+}$*Apoe*$^{-/-}$ and *Ccl17*$^{E/E}$*Apoe*$^{-/-}$ mice on high-fat diet using enzymatic digestion and FACS analysis. *$P < 0.05$.

EGFP+*Ccl17*$^{E/+}$ DCs, whereas EGFP− or unpulsed DCs elicited only marginal proliferative responses (Figure 4B). Notably, *Foxp3* mRNA expression was elevated in T cells cocultured with EGFP+*Ccl17*$^{E/E}$ DCs versus EGFP− or EGFP+*Ccl17*$^{E/+}$ DCs, which may indicate that the spontaneous differentiation of Tregs is limited in the presence of CCL17 (Figure 4B). Concurrently, we observed an increased percentage of apoptotic cells among proliferating but not resting OT-II CD4+ T cells (Figure 4B and data not shown).

Given the role of Jak/Stat signaling in regulating T cell growth and differentiation, we analyzed Stat phosphorylation patterns in proliferating OT-II CD4+ T cells by FACS. While Stat1, Stat3, and Stat6 phosphorylation did not differ (data not shown), Stat5 phosphorylation increased in OT-II CD4+ T cells interacting with OVA-2–pulsed EGFP+*Ccl17*$^{E/E}$ versus *Ccl17*$^{E/+}$ BMDCs (Figure 4B). OT-II Tregs exhibited higher numbers after coculture with OVA-2–pulsed *Ccl17*$^{E/E}$ versus *Ccl17*$^{+/+}$ BMDCs (Figure 4C). In contrast to effector CD4+ T cells, significantly fewer OT-II Tregs displayed signs of apoptosis after exposure to OVA-2–pulsed *Ccl17*$^{E/E}$ BMDCs, and phosphorylation levels of Stat5 differed only marginally (Figure 4C). Reduced frequencies of apoptotic Tregs were recapitulated in vivo in *Ccl17*$^{E/E}$ versus *Ccl17*$^{+/+}$ mice, but the rate of apoptosis in Foxp3−CD4+ T cells was unaltered (Figure 4D and data not shown). The frequencies of Tregs were significantly reduced by addition of recombinant CCL17 to anti-CD3–restimulated Tregs in the presence of IL-2 (Supplemental Figure 9A), indicating that CCL17 alone can interfere with signaling pathways mediating Treg maintenance.

To clarify the mechanisms of CCL17 action, namely a potential involvement of CCR4, we performed coculture experiments

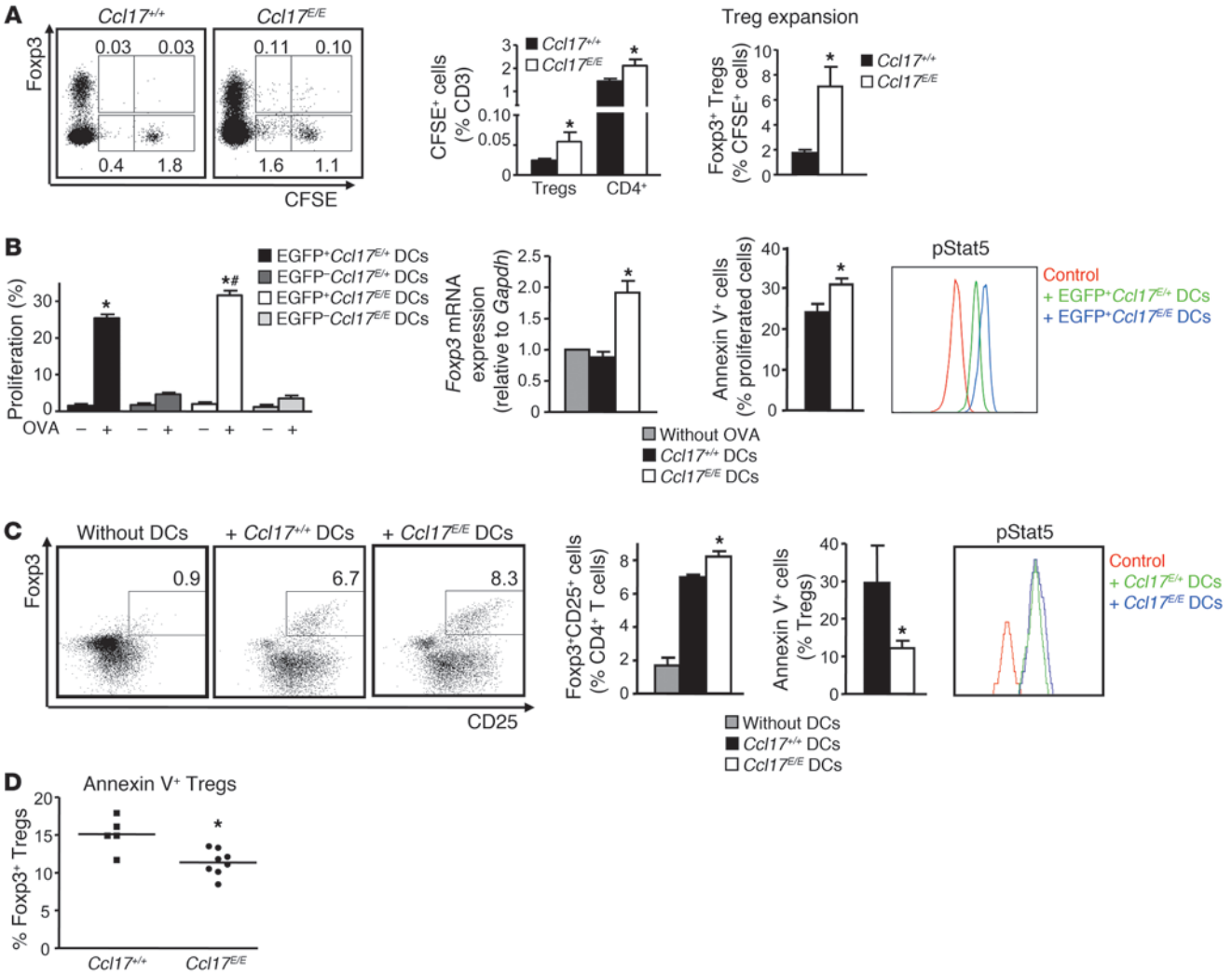

Figure 4

CCL17 controls the maintenance of Tregs. (**A**) CFSE-labeled CD4+CD25− T cells were transferred into *Ccl17*$^{+/+}$ or *Ccl17*$^{E/E}$ mice, and frequencies of CFSE+Foxp3+ Tregs and CFSE+CD4+ cells among T cells in LNs were analyzed by flow cytometry after 10 days. Representative dot plots and percentages within gates are shown ($n = 10$ per group). (**B**) Sorted unpulsed or OVA-2–pulsed EGFP− or EGFP+ *Ccl17*$^{E/+}$ or *Ccl17*$^{E/E}$ BMDCs were incubated with OT-II T cells in vitro ($n = 5$ independent experiments). T cell proliferation was quantified by CSFE dilution and FACS analysis after 3 days. OT-II T cells were back-sorted, and *Foxp3* mRNA expression was analyzed by real-time PCR. Frequencies of apoptotic annexin V+ cells were quantified by FACS analysis. *$P < 0.05$ versus unpulsed; #$P < 0.05$ versus OVA-pulsed EGFP+*Ccl17*$^{E/+}$ BMDCs. Phosphorylation of Stat5 (pStat5) was assessed by flow cytometry; representative histograms are shown. Fluorescence-minus-one measurements served as control. (**C**) OVA-2–pulsed *Ccl17*$^{+/+}$ or *Ccl17*$^{E/E}$ BMDCs were incubated with OT-II Tregs ($n = 3$ independent experiments). Frequencies of Foxp3+CD25+CD4+ and of annexin V+ Tregs among Foxp3+CD25+CD4+ Tregs were quantified by FACS analysis after 3 days; representative dot plots and percentage of Foxp3+CD25+ Tregs among CD4+ T cells within gates are shown. *$P < 0.05$ versus *Ccl17*$^{+/+}$ BMDCs. pStat5 was assessed by flow cytometry in Tregs; representative histograms are shown. (**D**) FACS analysis of annexin V+CD4+Foxp3+ Tregs in LNs of *Ccl17*$^{+/+}$ and *Ccl17*$^{E/E}$ mice. Data points represent frequencies of cells in individual mice; horizontal bars denote mean of all mice. *$P < 0.05$.

employing *Ccr4*$^{-/-}$ Tregs and BMDCs. Notably, the frequency of *Ccr4*$^{-/-}$ Tregs obtained in coculture with wild-type BDMCs was significantly higher than that of *Ccr4*$^{+/+}$ Tregs, paralleling higher frequencies of wild-type Tregs in cocultures with *Ccl17*$^{E/E}$ BMDCs (Supplemental Figure 9B). This implies that CCR4 on T cells is involved in mediating CCL17's effects on Treg maintenance, at least in vitro. In contrast, neutralization of the other CCR4 ligand, CCL22, using a blocking antibody did not affect Treg numbers in cocultures with wild-type BMDCs as compared with isotype control, identifying the regulation of Treg maintenance as a CCL17-specific function (Supplemental Figure 9B). Cocultures with *Ccr4*$^{-/-}$ BMDCs did not result in increased Treg frequencies (Supplemental Figure 9B), ruling out that the effect of CCL17 occurs in an autocrine fashion via CCR4.

Taken together, our data indicate that CCL17 expressed by a mature DC subset, also present in atherosclerotic lesions, suppresses expansion of Tregs by limiting their maintenance or conversion and promoting their apoptosis. Given the accumulation of

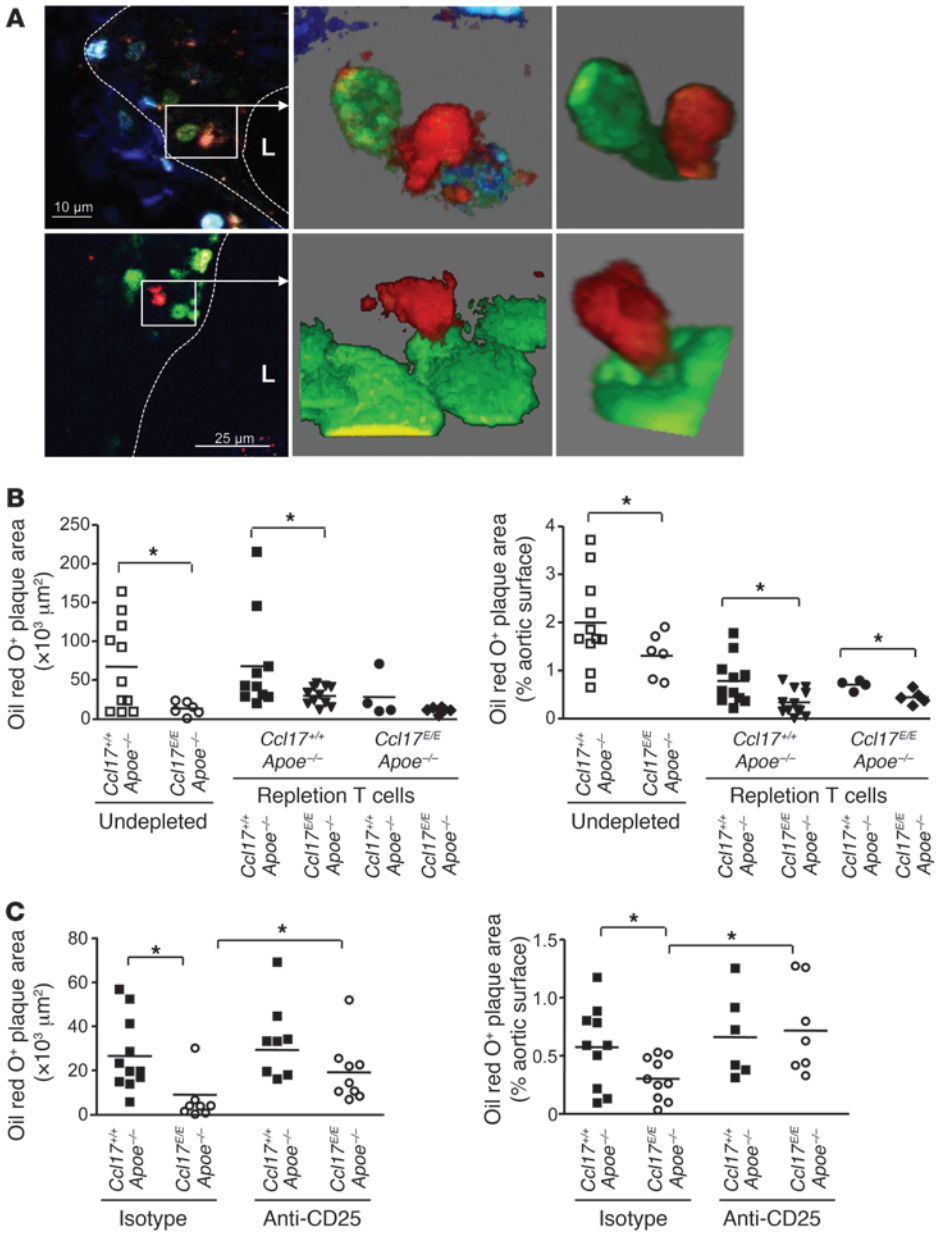

Figure 5
CCL17⁺ DCs mediate atherogenesis by priming T cells. (**A**) Multiphoton microscopy was used to obtain 2D optical slices (left images) and 3D projections of matching zoomed areas (middle and right images) revealing EGFP⁺ DCs (green cytoplasmic staining) in close contact with DiI-labeled CD4⁺ T cells (red) in atherosclerotic vessel walls at the carotid artery bifurcation (upper panels, ×10 μm) and the aortic root (lower panels, ×25 μm) of *Ccl17*$^{E/+}$*Apoe*$^{-/-}$ mice fed a high-fat diet. Dashed lines demarcate lesional area; L, lumen. (**B**) CD4⁺ T cells sorted from 6-month-old *Ccl17*$^{+/+}$ *Apoe*$^{-/-}$ and *Ccl17*$^{E/E}$*Apoe*$^{-/-}$ mice on normal chow were adoptively transferred into 8-week-old *Ccl17*$^{+/+}$*Apoe*$^{-/-}$ and *Ccl17*$^{E/E}$*Apoe*$^{-/-}$ mice depleted of CD4⁺ cells. Undepleted *Ccl17*$^{+/+}$*Apoe*$^{-/-}$ and *Ccl17*$^{E/E}$*Apoe*$^{-/-}$ mice served as controls. After 6 weeks of high-fat diet, atherosclerotic lesions were quantified in the aortic root and aorta after staining with oil red O. Individual data points represent average plaque area per mouse; horizontal bars denote mean. **P* < 0.05. (**C**) Atherosclerotic lesions were quantified in aortas stained with oil red O in *Ccl17*$^{+/+}$*Apoe*$^{-/-}$ and *Ccl17*$^{E/E}$ *Apoe*$^{-/-}$ mice treated with depleting anti-CD25 antibody or isotype control and fed a high-fat diet for 4 weeks. Individual data points represent average plaque area per mouse; horizontal bars denote mean. **P* < 0.05.

CCL17⁺ DCs at sites of inflammation and their localization within LNs (28), these finding suggest that CCL17⁺ DCs exert pivotal functions in shaping immune responses beyond the recruitment of T cells. We aimed to address whether these mechanisms may be relevant to DCs interacting with T cells in the vessel wall. Aortic CD11c⁺ DCs sorted from CD11c-EYFP mice and loaded with OVA triggered proliferation of OVA-specific OT-II CD4⁺ T cells in vitro (Supplemental Figure 10), corroborating the finding that vascular DCs can in principle prime antigen-specific T cell responses (30). Moreover, multiphoton microscopic analyses of atherosclerotic lesions were performed 3 days after transfer of labeled CD4⁺ T cells. Indeed, few CCL17⁺ DCs were observed in close vicinity and contact with CD4⁺ T cells in atherosclerotic aortic roots and carotid arteries of *Ccl17*$^{E/+}$*Apoe*$^{-/-}$ mice (Figure 5A), giving rise to the possibility that CCL17⁺ DCs may modulate T cell responses within the arterial wall characterized by atherosclerotic lesions.

T cells instructed by CCL17⁺ DCs mediate atherogenesis. To determine whether the DC-imprinted T cell signature (including an expansion of Tregs) arising in *Ccl17*$^{E/E}$*Apoe*$^{-/-}$ mice protects recipient *Apoe*$^{-/-}$ mice from atherosclerosis, CD4⁺ T cells from 6-month-old *Ccl17*$^{+/+}$*Apoe*$^{-/-}$ or *Ccl17*$^{E/E}$*Apoe*$^{-/-}$ mice that had been exposed to either CCL17⁺ DCs or CCL17-deficient DCs in vivo were adoptively transferred into 8-week-old *Apoe*$^{-/-}$ mice depleted of CD4⁺ cells using an anti-CD4 antibody (Figure 5B). Depleted *Apoe*$^{-/-}$ mice reconstituted with *Apoe*$^{-/-}$ T cells displayed slightly lower plaque size than nondepleted *Apoe*$^{-/-}$ controls, and the protective effect of CCL17 deficiency could be confirmed without treatment for T cell depletion (Figure 5B). Indeed, lesion formation was reduced in mice reconstituted with CD4⁺ T cells from *Ccl17*$^{E/E}$*Apoe*$^{-/-}$ mice, as compared with those receiving CD4⁺ T cells from *Ccl17*$^{+/+}$*Apoe*$^{-/-}$ mice (Figure 5B). Reconstitution of *Ccl17*$^{E/E}$*Apoe*$^{-/-}$ mice with CD4⁺ T cells from *Ccl17*$^{E/E}$*Apoe*$^{-/-}$ mice recapitulated the phenotype of

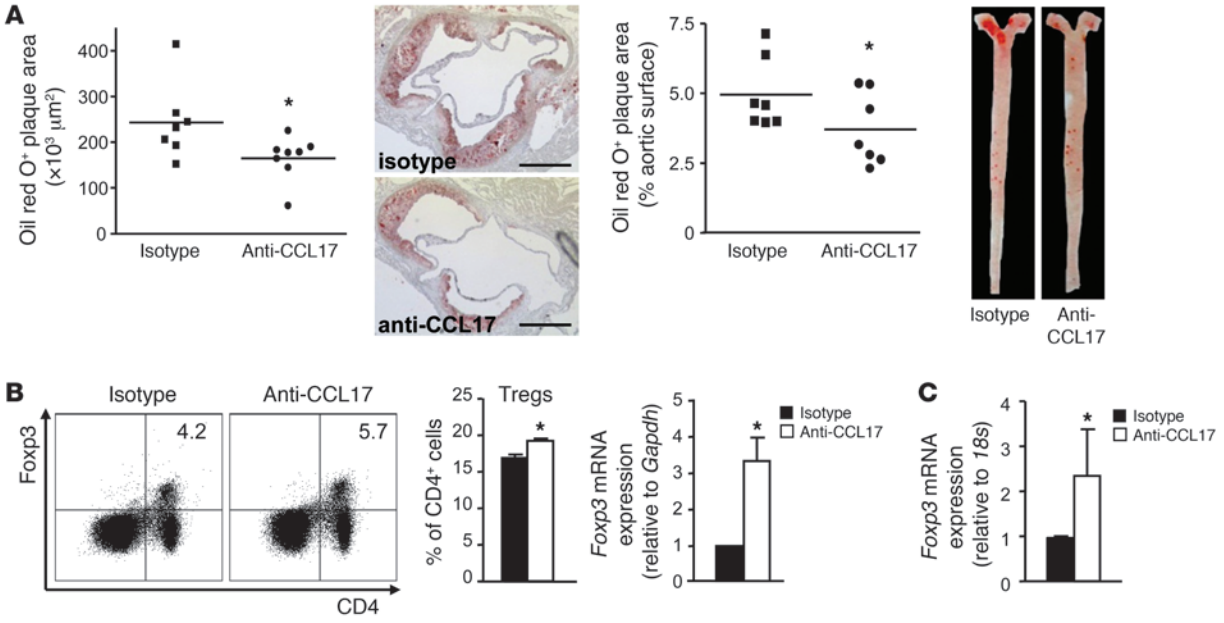

Figure 6

CCL17 as a potential therapeutic target. (**A**) *Apoe*$^{-/-}$ mice fed a high-fat diet for 4 weeks were injected with blocking antibody to CCL17 or isotype control for an additional 4 weeks. Atherosclerotic lesions were quantified in the aortic root (scale bars: 500 μm) and aorta after oil red O staining. Individual data points represent average plaque area per mouse; horizontal bars denote mean; representative images are shown. (**B**) Frequencies of CD4$^+$Foxp3$^+$ Tregs among CD3$^+$ cells in LNs were determined by flow cytometry; *Foxp3* mRNA levels in LNs by real-time PCR analysis. (**C**) Real-time PCR analysis of *Foxp3* mRNA expression in atherosclerotic aortas. *$P < 0.05$.

undepleted *Ccl17*$^{E/E}$*Apoe*$^{-/-}$ mice, and the transfer of *Ccl17*$^{+/+}$*Apoe*$^{-/-}$ CD4$^+$ T cells into *Ccl17*$^{E/E}$*Apoe*$^{-/-}$ recipients significantly increased atherosclerotic lesion size in the aorta; however, it resulted in a non-significant trend toward increased lesion size in the aortic root (Figure 5B), likely due to a partial re-adjustment of the donor T cell phenotype by exposure to CCL17-deficient DCs in recipient mice. Taken together, these data clearly demonstrate that T cells instructed by CCL17$^+$ DCs mediate the atherogenic effects.

In a reciprocal approach and to evaluate the functional contribution of CCL17-induced differences in Treg numbers, treatment with an anti-CD25 antibody depleting CD25$^+$ Tregs aggravated atherosclerosis in *Apoe*$^{-/-}$ controls and reversed the reduction in lesion formation and macrophage content in *Ccl17*$^{E/E}$*Apoe*$^{-/-}$ mice (Figure 5C and Supplemental Figure 11). Consistent with previous findings (31), this implies that T cells imprinted by DCs exert systemic effects on atherosclerosis and that the protective effects of *Ccl17* deficiency are mediated by Tregs.

CCL17 as a potential therapeutic target. To validate CCL17 as a therapeutic target in atherosclerosis, we employed a blocking antibody to CCL17 during disease progression. Treatment was initiated after 4 weeks of diet in *Apoe*$^{-/-}$ mice with early lesions and was continued for another 4 weeks of diet. Mice treated with anti-CCL17 displayed significantly reduced lesion formation and macrophage content in the aortic root and the aorta, compared with isotype control–treated *Apoe*$^{-/-}$ mice (Figure 6A and data not shown). This was accompanied by an expansion of Foxp3$^+$CD25$^+$ Tregs in LNs and increased levels of *Foxp3* mRNA in LNs of anti-CCL17–treated mice (Figure 6B). The expression of *Foxp3* mRNA was hardly detectable in aortas of *Apoe*$^{-/-}$ mice treated with isotype control but significantly elevated in anti-CCL17–treated *Apoe*$^{-/-}$ mice (Figure 6C), reflecting an increased presence of Treg in the aorta. These data indicate that targeting CCL17 may be a feasible therapeutic approach for treating established atherosclerosis.

Discussion

Here we report that deficiency in the DC-derived chemokine CCL17 entails a marked attenuation of atherosclerosis in *Apoe*$^{-/-}$ mice. Whereas the CD11c$^+$ DC network found in atherosclerosis-prone regions of naive mice does not express CCL17, we observed increased frequencies of EGFP$^+$CD11c$^+$ DCs in the aortic root of *Ccl17*$^{E/+}$ and *Ccl17*$^{E/E}$*Apoe*$^{-/-}$ mice during lesion evolution, paralleled by elevated *Ccl17* expression in advanced stages. In line with the detection of CCL17 and the presence of myeloid DCs at high numbers in advanced human plaques (8–10), *CCL17* transcripts were upregulated in human carotid endarterectomy specimens as compared with macroscopically healthy arteries. As evidenced by their presence in plaques of *Ccl17*$^{E/+}$ BM chimeras, CCL17$^+$ DCs or their precursors seem to be continuously recruited to growing lesions.

CCL17 expressed by mature DCs in the vessel wall may function to recruit T cells for instructive interactions. In conjunction with other pro-adhesive molecules expressed in plaques (32), it is conceivable that CCL17 immobilized and presented by endothelial cells (33) can participate in the recruitment of circulating T cells to atherosclerotic lesions, as shown for integrin-dependent arrest of memory T cells in chronically inflamed skin (34). Indeed, fewer CD3$^+$ T cells were observed in lesions of *Ccl17*$^{E/E}$*Apoe*$^{-/-}$ mice, and adoptively transferred CD4$^+$ T cells more efficiently homed to aortas of *Ccl17*$^{+/+}$*Apoe*$^{-/-}$ mice than to those of *Ccl17*$^{E/E}$*Apoe*$^{-/-}$ mice. In contrast, Treg recruitment was less pronounced and not altered in *Ccl17*$^{E/E}$*Apoe*$^{-/-}$ mice. Nevertheless, the inflammatory recruit-

ment of both CD4+ T cells and Tregs was enhanced by CCL17 in an air pouch model, providing direct evidence for a (non-preferential) role of CCL17 in Treg recruitment in an in vivo model of inflammation that differs from atherosclerosis, in line with previous studies showing that CCL17 enhances CD4+ T cell and Treg recruitment (25–27, 35). A minor or partial role of CCR4 in T cell accumulation in response to CCL17 in air pouches may be related to a predominant role of other receptors in this model of inflammation. Although the role of CCR4 in recruiting CD4+ T cells and Tregs toward CCL17 (and CCL22) has unequivocally been shown in vitro (25), lymphocyte and CD4+ T cell recruitment was unaltered in various in vivo models, e.g., OVA-induced airway inflammation, cardiac allograft rejection, and skin inflammation related to atopic dermatitis in *Ccr4*$^{-/-}$ mice (36–38). Notably, we found increased Treg accumulation in aortas of *Ccl17*$^{E/E}$*Apoe*$^{-/-}$ mice and in LNs of *Ccl17*-deficient mice. In conjunction with this finding, our data indicate that a higher Treg content is due not to selectively increased or preferential recruitment, which can occur independently of CCL17, but rather to effects on Treg maintenance.

Monitoring the fate of adoptively transferred T cells in *Ccl17*-deficient mice revealed an enhanced expansion or increased rate of conversion of Tregs and increased proliferation of CD4+ T cells and Tregs in vivo. In addition, antigen-specific interactions with *Ccl17*-deficient DCs led to increased proliferation of CD4+ T cells but also their apoptosis, possibly related to activation-induced cell death or T cell exhaustion. Antigen-specific interactions with *Ccl17*$^{E/E}$ DCs enhanced the maintenance of Tregs but — in a striking contrast to CD4+ T cells — this was accompanied by reduced apoptosis. The profound bias favoring Treg maintenance was confirmed in *Ccl17*-deficient *Apoe*$^{-/-}$ mice in vivo, where the rate of apoptosis was reduced in Tregs but unaltered in CD4+ T cells. Notably, Stat5 phosphorylation was increased in proliferating CD4+ T cells and slightly enhanced in Tregs after interaction with antigen-presenting *Ccl17*$^{E/E}$ DCs. The proliferation of T cells is tightly regulated by Stat5, which is recruited to the TCR in response to stimulation (39). Whereas *Stat5*$^{-/-}$ mice display decreased T cell proliferation due to defective expression of the IL-2 receptor α-chain (40), constitutive overexpression of the active form of Stat5 was found to enhance T cell proliferation but also the rate of apoptosis (41). Accordingly, the increased activation of Stat5 may interfere with IL-2 production and subsequently induce a negative feedback signal in CD4+ T cells with elevated sensitivity to cell death (42–46). Moreover, a marked expansion of Tregs was observed in mice with constitutive overexpression of active Stat5 (41). Given the importance of IL-2 in STAT5 activation to sustain Foxp3 expression in Tregs, involving STAT5 binding to a highly conserved STAT-binding site located in the first intron of the *FOXP3* gene (47), interference with Stat5 may not only constrict T cell proliferation but also diminish conversion into Foxp3+ Tregs and their peripheral maintenance. Although the pathways involved in CCL17's effects remain to be elucidated, mechanisms inhibiting Jak/Stat signaling are well defined, e.g., dephosphorylation, proteolytic degradation, or association with inhibitory molecules (48). It is conceivable that CCL17 can interfere with Stat5 phosphorylation by inducing the MAPK pathway, as seen for CCL17-induced interference with Src kinase and ERK phosphorylation, or the PI3K pathway (49–51). Notably, the putative Stat-inducible gene *c-fos* was upregulated in T cells after exposure to *Ccl17*$^{E/E}$ DCs (A. Zernecke et al., unpublished observations), supporting the hypothesis that CCL17 interacts with growth and differentiation processes through a Stat-dependent pathway.

Although *Ccr4*$^{-/-}$ Treg frequencies obtained in coculture with BMDCs were higher than those of *Ccr4*$^{+/+}$ Tregs — suggesting that in vitro CCR4 on T cells is involved in mediating CCL17's effects on Treg maintenance — deficiency in *Ccr4* did not phenocopy the effects of *Ccl17* deficiency in other assays. No alterations in frequencies of transferred *Ccr4*$^{-/-}$ CD4+ T cells or in expanded or converted *Ccr4*$^{-/-}$ Tregs or the prevalence of CD4+ T cells and Tregs in *Ccr4*$^{-/-}$ mice were observed. Thus, the mechanisms enacted by CCL17 are not solely mediated by CCR4, clearly implying the contribution of other receptors to the complex functional profile of CCL17. This would also explain why, unlike the deletion of *Ccl17*, a lack of *Ccr4* in BM-derived cells did not confer protection against the formation of atherosclerotic lesions, which likely requires an attenuation of the full scope and spectrum of CCL17-mediated actions.

Tregs are instrumental for maintaining self tolerance and preventing uncontrolled inflammation or autoimmune disease (52). Whereas natural Foxp3+ T cells arise in the thymus, Tregs expressing Foxp3 develop from conventional T cells in the peripheral immune compartment in the absence of inflammatory stimuli. Distinct antigen-presenting cell subsets have been identified to induce Tregs, e.g., in the intestinal lamina propria and spleen (53). Conversely, cell types crucial in the restriction or retraction of Treg responses have not been defined. Here we provide the first evidence to our knowledge that CCL17+ DCs control the maintenance of Tregs and that chemokines, namely CCL17, can crucially determine the T cell phenotype. This extends findings that chemokines can control cell homeostasis beyond recruitment, thus epitomizing non-chemotactic functions of chemokines (54). Our transfer studies further indicate that immune responses in T cells initiated and sustained by interactions with CCL17+ DCs are essential for orchestrating atheroprogression, extending data that CD4+ T cells can elicit atherosclerosis in immunodeficient *Apoe*$^{-/-}$ mice (31). We also demonstrate that a Treg expansion in the absence of CCL17+ DCs protects mice from lesion formation, in line with reports that Tregs act as powerful inhibitors of atherosclerosis (18, 21).

It remains to be determined whether immune responses are initiated and sustained in the arterial wall or in secondary lymphatic tissue. Here we confirm that vascular CD11c+ DCs sorted from the aorta in principle bear the capacity to induce antigen-specific proliferation of CD4+ T cells in vitro (30). Moreover, an oligoclonal expansion of T cells can be found in the vessel wall (55), implying that priming of T cells or re-encounter of antigen may also occur locally at sites of inflammation. Moreover, CCL17+ DCs elicited strong T cell proliferative responses when compared with CCL17− DCs, consistent with previous findings (28). Although OVA was used as an artificial antigen irrelevant to atherosclerosis in these assays, these data add to our principal understanding of this DC subset and the function of CCL17, which may be translatable to atherosclerosis. DCs within the vessel wall may thus also modulate T cell responses within plaques. Although CCL17+ DCs can be localized in close proximity to CD4+ T cells within lesions and some proliferating CD4+ T cells are present within lesions, only few Tregs are detectable in atherosclerotic plaques. Together with the marginal recruitment of Tregs to the inflamed aorta, this implies that CCL17+ DCs may be involved in homeostatic mechanisms primarily within lymphoid tissue. Thus, it is likely that the primary site for Treg formation is secondary lymphoid tissue, from which Tregs may be recruited to sites of inflammation at low numbers. A withdrawal of suppressive effects exerted by lesional Tregs may sustain inflammation and exacerbate plaque growth. Further to

systemic effects, Tregs can skew monocyte/macrophage activation toward a "regulatory" phenotype, which may limit atheroprogression by secretion of antiinflammatory cytokines (56, 57). In turn, alternative macrophages can propagate Treg differentiation (58) to enhance atheroprotection.

Although the egress of immune cells from the aortic wall appears minimal during progressive disease, emigration of cells from tissue is considered to be a hallmark of DCs (59). Beyond local vascular effects, CCL17$^+$ DCs may also travel to regional LNs after antigen uptake and activation. Here we provide the first evidence to our knowledge that aortic CD11c$^+$ and CCL17$^+$ DCs displaying high expression levels of CCR7 share the capacity to migrate to regional LNs after footpad injection or directly from transplanted *Ccl17*$^{E/+}$ or *Ccl17*$^{E/E}$ aortas. Whereas CCL17 is required to sensitize DCs for CCR7- or CXCR4-dependent emigration from skin in atopic dermatitis, translating into migratory defects of *Ccl17*$^{E/E}$ DCs (38), the accumulation of EGFP$^+$ DCs in atherosclerotic arteries or in LNs after footpad injection was not substantially affected by CCL17 itself. Although DCs migrating to LNs from the footpad do not mimic the pathophysiology of the arterial intima and aortic transplantation may cause a local inflammatory response, the finding that CCL17$^+$ DCs originating from atherosclerotic aortas can travel to regional LNs may support the concept that these cells are more likely to exert their function through systemic effects in secondary lymphatic tissue. Moreover, during hypercholesterolemia, DCs as well as CCL17$^+$ DCs can be sequestered in the periphery (60) and may thus present antigens such as oxLDL- or LDL-derived peptides in lymphoid tissue. Notably, a recent study employing *Ccr7*$^{-/-}$ mice provided evidence supporting the hypothesis that local priming processes in the inflamed vessel wall or lymphoid tissue alone are insufficient to generate or maintain an adaptive immune response promoting atherogenesis; and that CCR7-dependent trafficking of T cells to draining LNs and their (re)entry to sites of inflammation are essential (61).

Taken together, our findings indicate that CCL17$^+$ DCs may regulate homeostatic mechanisms in T cells primarily in lymphoid tissue. Given that fewer CD3$^+$ T cells were observed in lesions of *Ccl17*$^{E/E}$*Apoe*$^{-/-}$ mice and that adoptively transferred CD4$^+$ T cells homed more efficiently to aortas of *Ccl17*$^{+/+}$*Apoe*$^{-/-}$ mice than to those of *Ccl17*$^{E/E}$*Apoe*$^{-/-}$ mice, CCL17$^+$ DCs in atherosclerotic plaques may function to recruit T cells (instructed in the LN) to the vessel wall to promote inflammation. The increased Treg accumulation in atherosclerotic aortas of *Ccl17*-deficient mice further implies that lesional CCL17$^+$ DCs may contribute to homeostatic mechanisms at the site of inflammation. Thus, CCL17 expressed in atherosclerotic plaques may also serve to locally constrain Treg maintenance to some extent, thereby propagating inflammation. These findings are in line with a growing body of evidence pointing toward a proinflammatory role of CCL17, as demonstrated by ameliorated contact hypersensitivity and survival of cardiac allografts in *Ccl17*$^{-/-}$ mice (28, 38).

In conclusion, CCL17 characterizes a DC subset that is of paramount importance in the initiation and progression of atherosclerosis. Not only do CCL17$^+$ DCs have the unique capacity to recruit or retain inflammatory T cells at sites of lesion growth, but they also limit Treg maintenance in lymphatic tissue. These data establish that DC-specific effector functions regulated by CCL17 are crucial in the pathogenesis of atherosclerosis. The elevated expression of *CCL17* in human atherosclerosis underscores the possible clinical relevance of our findings. As illustrated by the inhibitory effects of an antibody to CCL17 on atheroprogression, DC-derived CCL17 may represent an attractive molecular target that can be translated into new therapeutics for preventing atheroprogression and treating advanced atherosclerosis (62).

Methods

Mouse models and BM transplantation. CD11c-EYFP mice (63) were provided by M. Nussenzweig (Rockefeller University, New York, New York, USA). *Ccr4*$^{-/-}$ mice (36) were from K. Pfeffer (Heinrich-Heine-Universität, Düsseldorf), and *Apoe*$^{-/-}$ and *Ldlr*$^{-/-}$ mice were obtained from The Jackson Laboratory. *Foxp3gfp.KI* mice were previously described (64). *Ccl17*$^{E/E}$ mice (28) were crossed with *Apoe*$^{-/-}$ mice (all C57BL/6J background). Female *Apoe*$^{-/-}$, *Ccl17*$^{E/+}$*Apoe*$^{-/-}$, and *Ccl17*$^{E/E}$*Apoe*$^{-/-}$ littermates were fed normal chow. At 8 weeks of age, some mice were placed on atherogenic diet (21% fat, 0.15% cholesterol, Altromin). BM transplantations were performed as described previously (65). Briefly, BM cells (5×10^6 in PBS) from donor mice were administered to recipient mice by intravenous tail vein injection 24 hours after an ablative dose of whole-body irradiation (2×6.5 Gy). Some 8-week-old female *Apoe*$^{-/-}$ mice were placed on an atherogenic diet and after 4 weeks were treated intraperitoneally with an anti-murine CCL17 antibody (200 μg/injection, 3 times/wk, rat IgG2a, R&D Systems) or corresponding isotype control antibody (200 μg/injection, 3 times/wk, rat IgG2a, BioXcell) for an additional 4 weeks of diet. Circulating rat antibodies were detectable both in serum of *Apoe*$^{-/-}$ mice injected with isotype control or anti-CCL17 antibody 3 days after the first injection and 3 days after the last injection after treatment for 4 weeks, although a reduction possibly due to immunoclearance was observed (8,529 ± 2,493 ng/ml after 3 days vs. 820 ± 164 ng/ml rat IgG after 4 weeks, threshold 155 ± 5 ng/ml). Given a typical median neutralization dose (ND_{50}) of 750 ng/ml for the anti-CCL17 antibody, these values are indicative of efficient neutralization during this period. Some 8-week-old *Apoe*$^{-/-}$ mice were treated intraperitoneally with 2 doses of anti-mouse CD4 depleting antibody (300 μg/injection, GK1.5, BioLegend) 7 and 4 days before adoptive transfer of 5×10^6 CD4$^+$ T cells by tail vein injection, resulting in less than 0.5% CD4$^+$ T cells among CD45$^+$ cells in LNs. Upon transfer, all groups of mice were equally reconstituted with the following frequencies of CD4$^+$ T cells among CD45$^+$ cells: 12.7% ± 1.0% versus 13.5% ± 1.2% in *Ccl17*$^{+/+}$*Apoe*$^{-/-}$ mice repleted with T cells from *Ccl17*$^{+/+}$*Apoe*$^{-/-}$ and *Ccl17*$^{E/E}$*Apoe*$^{-/-}$ mice, 16.4% ± 1.5% versus 18.0% ± 1.6% in *Ccl17*$^{E/E}$*Apoe*$^{-/-}$ mice repleted with T cells from *Ccl17*$^{+/+}$*Apoe*$^{-/-}$ and *Ccl17*$^{E/E}$*Apoe*$^{-/-}$ mice, respectively; NS). Donor CD4$^+$ T cells were isolated from secondary lymphoid organs by negative immunomagnetic separation using a CD4$^+$ T cell isolation kit II (Miltenyi). Some high-fat diet–fed *Ccl17*$^{+/+}$*Apoe*$^{-/-}$ or *Ccl17*$^{E/E}$*Apoe*$^{-/-}$ littermates were intraperitoneally injected with a depleting anti-CD25 antibody or isotype control (clone PC61, Bioceros or Bioxcell), efficiently depleting Tregs with marginal effects on effector T cells in LNs or blood, as evident after 4 weeks of injections and 1 week after the last injection (Supplemental Figure 12). Lipid levels were unaltered in all groups (Supplemental Table 1). Experiments were approved by local authorities (Landesamt für Natur, Umwelt und Verbraucherschutz Nord-rhein-Westfalen, Recklinghausen, Germany) and complied with German animal protection law.

Multiphoton microscopy. Carotid arteries were mounted in a perfusion chamber and imaged using a Bio-Rad 2100MP (66) or a LaVision Trimscope multiphoton system coupled to an Olympus BX61WI microscope. Aortas were opened longitudinally through to the aortic valve region and embedded in agarose gel (1.5% in HBSS). Excitation lasers (Bio-Rad: Spectra-Physics Tsunami; LaVision: MaiTai HP) were tuned at 840 nm to visualize EYFP and second harmonic generation of collagen (SHG) or 800 nm to visualize EGFP and fluorescent probes. A Nikon ×60 (NA 1.0; water dipping) or an Olympus ×20 (NA 0.95; water dipping) objective was

used. An increase in magnification was achieved by internal optical zoom (Bio-Rad) or by reducing the field of view while maintaining pixel resolution (LaVision). For detection of emitted fluorescent signals, 3 photo multiplier tubes (PMTs) were tuned to corresponding parts of the emission spectra of fluorescent markers: SHG 400–470 nm (PMT1); Syto 41 (Molecular Probes, Invitrogen), 470–480 nm (PMT1); EGFP, 500–550 nm (PMT2); YFP, 530–560 nm (PMT2); MHC-II–PE (eBioscience), 560–600 nm (PMT3); propidium iodide (PI), 560–600 nm (PMT3); and CellTracker CM-DiI (both Molecular Probes, Invitrogen), 560–620 nm (PMT3). For simultaneous imaging of a combination of fluorescent markers, each PMT was tuned for minimal bleed-through. Separate images of 512 × 512 pixels (Bio-Rad) or 1,024 × 1,024 pixels (LaVision) were obtained from each PMT and combined into single RGB images. Images were collected in *xy* directions, and series of *xy* images were obtained at successive 1-μm-depth positions (*z*-stack) for reconstruction of 3D images. Image analysis was performed using Image-Pro Analyzer 7.0 (Media Cybernetics).

Aortic transplantation. Murine infrarenal aortic isografts were orthotopically transplanted into *Apoe*$^{-/-}$ mice. The abdominal aortic transplantation was performed as described previously using the sleeve technique (67). The mean surgical anastomosis time was 22 minutes (range, 13–40 minutes).

Quantification and immunohistochemical analysis of atherosclerosis. The extent of atherosclerosis was assessed in aortic roots and on thoracoabdominal aortas by staining for lipid depositions with oil red O (65, 68) and quantified by computerized image analysis (Diskus Software, Hilgers) and Leica Qwin Imaging software. Briefly, atherosclerotic lesions were measured in 5-μm transverse sections through the heart and the aortic roots. The thoracoabdominal aorta was opened longitudinally, and the percentage of lipid deposition was calculated by dividing the stained area by the total thoracoabdominal aortic surface. The relative content of macrophages, CD3$^+$ T cells, and SMCs (65) was determined by mAb staining for MOMA-2 (MCA519), CD3 (MCA1477, both Serotec), and smoothelin (N-15, Santa Cruz Biotechnology Inc.) and detection with Cy3-conjugated antibody (Jackson ImmunoResearch Laboratories Inc.). Nuclei were counterstained by DAPI. Images were recorded with a Leica DMLB fluorescence microscope and CCD camera.

BMDC culture. DCs were cultured from BM-derived Flt3$^+$ progenitor cells (69). Femurs and tibias were removed aseptically from donor mice, marrow cavities were flushed, and BM cell suspensions seeded at 2 × 10^6 cells/ml in RPMI-1640 medium supplemented with 10% FCS, L-glutamine (2 mM), penicillin/streptomycin (100 U/ml), β-mercaptoethanol (50 μM, Sigma-Aldrich), murine rSCF (30 U/ml), Flt-3L (25 ng/ml), murine GM-CSF (25 U/ml, all PeproTech), rIL-6/soluble IL-6R fusion protein (5 ng/ml, hyper–IL-6; a gift from S. Rose-John, Christian-Albrechts-Universität, Kiel, Germany), long-range rIGF-1 (40 ng/ml), and 10^{-6} M dexamethasone (both Sigma-Aldrich). After 3 days, cells were subjected to Ficoll-Hypaque density gradient (1.077 g/ml; Eurobio) centrifugation. After 7 days, differentiation of Flt3$^+$ progenitor cells into DCs was induced with 250 U/ml GM-CSF.

Enzymatic tissue digestion, flow cytometry, cell sorting, and ELISA. For FACS analyses, tissues and LNs were dissociated into single-cell suspensions with collagenase D (Roche) for 30 minutes at 37°C. Aortas were excised, flushed in PBS, and digested using Liberase III (Roche). Staining for flow cytometric analysis was conducted using combinations of antibodies from BioLegend (MHC-II), Cell Signaling Technology (pSTAT1, -3, -5), eBioscience (CD11c, CD11b, CD115, B220, CD8a, 440c, CD24, CD69, CD80, CD86, CD40, CD3, CD4, CD44, CD62L, CD25, CD45, Foxp3, MHC-II, TNF-α), and BD (GR-1) in HBSS with 0.3 mM EDTA and 0.1% BSA. Intracellular labeling of Foxp3, Stat phosphorylation, and TNF-α was performed according to the manufacturers' protocols. Probes were analyzed in a FACSCanto II, and sorting was performed using a BD FACSAria (BD) and FlowJo software (Tree Star). Serum cytokines were analyzed using mouse IL-10 and IFN-γ Quantikine ELISA Kits (R&D Systems). Antibodies to malondialdehyde-modified LDL were measured by chemiluminescence ELISA (16). Circulating rat antibodies were determined using a quantitative rat IgG ELISA Kit (Alpha Diagnostics International).

Transmigration and in vivo cell recruitment. The migration of CD11c$^+$ vascular DCs, sorted from digested aorta tissue of CD11-EYFP mice (5 × 10^5), and sorted EGFP$^+$*Ccl17*$^{E/+}$ and EGFP$^+$*Ccl17*$^{E/E}$ DCs (5 × 10^6) was assessed 18 hours after injection into the footpad of recipient C57BL/6 mice by flow cytometry of peripheral LN cells. CD4$^+$ T cells were isolated by immunomagnetic separation using CD4 microbeads (Miltenyi Biotec) from spleen and LNs of C57BL/6 or OT-II mice. For T cell homing assays, 5 × 10^6 isolated and CFSE-labeled CD4$^+$ T cells (CFSE, Fluka) or allophycocyanin-labeled (APC-labeled) isolated Tregs (CD4$^+$CD25$^+$ T Cell Isolation Kit, Miltenyi Biotec; cell proliferation dye eFluor 670, eBioscience) were injected intravenously into *Ccl17*$^{+/+}$, *Ccl17*$^{E/E}$, *Ccl17*$^{+/+}$*Apoe*$^{-/-}$, or *Ccl17*$^{E/E}$*Apoe*$^{-/-}$ mice. Recruitment to peripheral LNs or aortas was assessed by FACS analysis after 2 hours and 3 days, respectively. Sorted EGFP$^+$*Ccl17*$^{E/+}$ and EGFP$^+$*Ccl17*$^{E/E}$ DCs (2 × 10^5) were added to 48-well tissue culture plates at a final volume of 600 μl RPMI-1640 medium containing 0.5% BSA. Isolated CD4$^+$ T cells (2 × 10^5) were added to upper chambers of Transwell inserts (Costar, 3-μm pore size). After 2 hours at 37°C, migrated cells were quantified after staining by flow cytometry as percentage of input. To analyze in vivo recruitment of CD4$^+$ T cells, we created a subcutaneous air pouch by injection of 5 ml of sterile air at days 0 and 4 (70). At day 7, mouse CCL17 (R&D Systems, in 1 ml sterile PBS) or PBS was injected into the pouch. At different time points, the pouch was lavaged with 5 mM EDTA in HBSS. Single-cell suspensions were stained and quantified by flow cytometry.

Antigen-specific T cell proliferation. CD4$^+$ T cells were isolated from spleens of OT-II mice by CD4 microbeads (Miltenyi Biotec) and labeled with CFSE (Fluka). DCs were pulsed for 30 minutes with 1 μg/ml with $OVA_{323–339}$ peptide (ISQAVHAAHAEINEAGR, OVA-2, ANASPEC) for MHC-II–restricted T cell stimulation. Untreated DCs served as control. In vivo, 5 × 10^6 CD4$^+$ CFSE-labeled OT-II cells were injected into tail veins of C57BL/6 recipient mice. One day later, 5 × 10^6 untreated or OVA-2–pulsed DCs were injected into the footpad. After 3 days, single-cell suspensions were prepared from peripheral LNs of recipient mice to analyze T cell proliferation. In vitro, a total of 3 × 10^4 OT-II T cells or Tregs were cocultured with 10^4 DCs in 200 μl of medium containing GM-CSF in 96-well flat-bottom microtiter plates for 72 hours at 37°C. T cell proliferation was analyzed by CFSE dye dilution after 3 days by flow cytometry.

Treg polarization, restimulation, and conversion assays. Naive CD4$^+$ spleen and LN cells were obtained by immunomagnetic isolation (Miltenyi Biotec). CD4$^+$ T cells (5 × 10^5) were cultured in 24-well tissue culture plates in 1 ml DC medium in the presence of 3 μg/ml anti-CD3e (clone 145-2C11) and supplemented with TGF-β (4 ng/ml) for 3 days. In vitro polarized Tregs were restimulated with anti-CD3e (5 μg/ml) and IL-2 (50 U/ml) for 2 days. CD4$^+$CD25$^-$ T cells were sorted from LNs and spleens, labeled with CFSE, and transferred intravenously. After 10 days, mice were sacrificed and LNs isolated and processed for flow cytometry.

Quantitative real-time PCR. RNA was isolated from LNs and aortas by TRIzol (Invitrogen). cDNA was reverse transcribed from 2 μg of DNase-treated total RNA (Promega). RNA was isolated from aortic sections using the Pinpoint Slide RNA Isolation system (Zymo Research) and amplified using ExpressArt TRinucleotide mRNA amplification Nano kit (amsbio). Reverse transcription of amplified RNA was performed with a TaqMan Reverse Transcription Kit, and real-time PCR analysis was performed using Pre-Developed TaqMan assays for mGAPDH (4352932E), m18s (4333760), and mFoxp3 (Mm00475165_m1, both Applied Biosystems) according to manufacturers' protocols in a thermal cycler 7900HT (Applied Biosystems) or SYBR Green RT-PCR system (BD Biosciences — Clontech) with specific

primer pairs (Sigma-Aldrich): *Ifng*: 5′-TGGCTCTGCAGGATTTTCAT-3′, 5′-TCAAGTGGCATAGATGTGGA-3′; *Il10*: 5′-TGCACTACCAAAGCCACAAGG-3′, 5′-TGGGAAGTGGGTGCAGTTATTG-3′; *Foxp3*: 5′-TTGGTTTACTCGCATGTTCG-3′, 5′-AGGGATTGGAGCAGCACTTGTTG-3′; *Gapdh*: 5′-CCATCACCATCTTCCAGGAG-3′, 5′-GTGGTTCACACCCATCACAA-3′. Amplification (45 cycles, annealing at 58°C) was performed in duplicate using an MJ Research Opticon 2 (Biozym).

Statistics. Data represent mean ± SEM and were analyzed by 2-tailed Student's *t* test, ANOVA with Newman-Keuls or Dunnett's multiple comparison test, or nonparametric Mann-Whitney *U* or Kruskal-Wallis test (Prism 4.0 software, GraphPad), as appropriate. Differences with *P* values less than 0.05 were considered to be statistically significant.

Acknowledgments

We thank X. Ren for help with experiments and M. Garbe, S. Roubrocks, M. Schott, and S. Wilbertz for excellent technical assistance. This work was supported by the Interdisciplinary Centre for Clinical Research Aachen (to A. Zernecke) and the Deutsche Forschungsgemeinschaft (FOR809, WE1913/11-1 and 11-2 to C. Weber; SFB704 TPA1 to I. Förster; ZE827/1-1 to A. Zernecke, T. Hieronymus, and M. Zenke; ZE827/1-2 to A. Zernecke and M. Zenke; SFB688 TPA12 and ZE827/4-1 to A. Zernecke).

Received for publication August 27, 2010, and accepted in revised form April 13, 2011.

Address correspondence to: Alma Zernecke, Rudolf-Virchow-Zentrum/DFG–Forschungszentrum für Experimentelle Biomedizin der Universität Würzburg, Joseph-Schneider-Str. 2, Haus D15, 97080 Würzburg, Germany. Phone: 49.0.931.31.80373; Fax: 49.0.931.31.83255; E-mail: alma.zernecke@virchow.uni-wuerzburg.de. Or to: Christian Weber, Institut für Prophylaxe und Epidemiologie der Kreislaufkrankheiten, Klinikum der Universität München, Ludwig-Maximilians-Universität, Pettenkoferstr. 9, 80336 Munich, Germany. Phone: 49.89.5160.4350; Fax: 49.89.5160.4352; E-mail: christian.weber@med.uni-muenchen.de.

1. Hansson GK, Libby P. The immune response in atherosclerosis: a double-edged sword. *Nat Rev Immunol*. 2006;6(7):508–519.
2. Weber C, Zernecke A, Libby P. The multifaceted contributions of leukocyte subsets to atherosclerosis: lessons from mouse models. *Nat Rev Immunol*. 2008; 8(10):802–815.
3. Shortman K, Naik SH. Steady-state and inflammatory dendritic-cell development. *Nat Rev Immunol*. 2007;7(1):19–30.
4. Zenke M, Hieronymus T. Towards an understanding of the transcription factor network of dendritic cell development. *Trends Immunol*. 2006;27(3):140–145.
5. Millonig G, et al. Network of vascular-associated dendritic cells in intima of healthy young individuals. *Arterioscler Thromb Vasc Biol*. 2001;21(4):503–508.
6. Jongstra-Bilen J, Haidari M, Zhu SN, Chen M, Guha D, Cybulsky MI. Low-grade chronic inflammation in regions of the normal mouse arterial intima predisposed to atherosclerosis. *J Exp Med*. 2006; 203(9):2073–2083.
7. Liu P, et al. CX3CR1 deficiency impairs dendritic cell accumulation in arterial intima and reduces atherosclerotic burden. *Arterioscler Thromb Vasc Biol*. 2008; 28(2):243–250.
8. Bobryshev YV. Dendritic cells in atherosclerosis: current status of the problem and clinical relevance. *Eur Heart J*. 2005;26(17):1700–1704.
9. Yilmaz A, et al. Emergence of dendritic cells in rupture-prone regions of vulnerable carotid plaques. *Atherosclerosis*. 2004;176(1):101–110.
10. Greaves DR, et al. Linked chromosome 16q13 chemokines, macrophage-derived chemokine, fractalkine, and thymus- and activation-regulated chemokine, are expressed in human atherosclerotic lesions. *Arterioscler Thromb Vasc Biol*. 2004;21(6):923–929.
11. Paulson KE, Zhu SN, Chen M, Nurmohamed S, Jongstra-Bilen J, Cybulsky MI. Resident intimal dendritic cells accumulate lipid and contribute to the initiation of atherosclerosis. *Circ Res*. 2010;106(2):383–390.
12. Alderman CJ, Bunyard PR, Chain BM, Foreman JC, Leake DS, Katz DR. Effects of oxidised low density lipoprotein on dendritic cells: a possible immunoregulatory component of the atherogenic microenvironment? *Cardiovasc Res*. 2002;55(4):806–819.
13. Packard RR, Maganto-Garcia E, Gotsman I, Tabas I, Libby P, Lichtman AH. CD11c(+) dendritic cells maintain antigen processing, presentation capabilities, and CD4(+) T-cell priming efficacy under hypercholesterolemic conditions associated with atherosclerosis. *Circ Res*. 2008;103(9):965–973.
14. Hansson GK. Inflammation, atherosclerosis, and coronary artery disease. *N Engl J Med*. 2005; 352(16):1685–1695.
15. Kleemann R, Zadelaar S, Kooistra T. Cytokines and atherosclerosis: a comprehensive review of studies in mice. *Cardiovasc Res*. 2008;79(3):360–376.
16. Binder CJ, et al. IL-5 links adaptive and natural immunity specific for epitopes of oxidized LDL and protects from atherosclerosis. *J Clin Invest*. 2004; 114(3):427–437.
17. Mallat Z, et al. Protective role of interleukin-10 in atherosclerosis. *Circ Res*. 1999;85(8):e17–e24.
18. Ait-Oufella H, et al. Natural regulatory T cells control the development of atherosclerosis in mice. *Nat Med*. 2006;12(2):178–180.
19. Taleb S, et al. Loss of SOCS3 expression in T cells reveals a regulatory role for interleukin-17 in atherosclerosis. *J Exp Med*. 2009;206(10):2067–2077.
20. van Es T, et al. Attenuated atherosclerosis upon IL-17R signaling disruption in LDLr deficient mice. *Biochem Biophys Res Commun*. 2009;388(2):261–265.
21. Gotsman I, et al. Impaired regulatory T-cell response and enhanced atherosclerosis in the absence of inducible costimulatory molecule. *Circulation*. 2006;114(19):2047–2055.
22. Gautier EL, et al. Macrophage apoptosis exerts divergent effects on atherogenesis as a function of lesion stage. *Circulation*. 2009;119(13):1795–1804.
23. Birnberg T, et al. Lack of conventional dendritic cells is compatible with normal development and T cell homeostasis, but causes myeloid proliferative syndrome. *Immunity*. 2008;29(6):986–997.
24. Habets KL, et al. Vaccination using oxLDL-pulsed dendritic cells reduces atherosclerosis in LDL receptor-deficient mice. *Cardiovasc Res*. 2010; 85(3):622–630.
25. Sallusto F, Mackay CR, Lanzavecchia A. The role of chemokine receptors in primary, effector, and memory immune responses. *Annu Rev Immunol*. 2000; 18:593–620.
26. Iellem A, et al. Unique chemotactic response profile and specific expression of chemokine receptors CCR4 and CCR8 by CD4(+)CD25(+) regulatory T cells. *J Exp Med*. 2001;194(6):847–853.
27. Andrew DP, et al. C-C chemokine receptor 4 expression defines a major subset of circulating nonintestinal memory T cells of both Th1 and Th2 potential. *J Immunol*. 2001;166(1):103–111.
28. Alferink J, et al. Compartmentalized production of CCL17 in vivo: strong inducibility in peripheral dendritic cells contrasts selective absence from the spleen. *J Exp Med*. 2003;197(5):585–599.
29. Fisson S, et al. Continuous activation of autoreactive CD4+ CD25+ regulatory T cells in the steady state. *J Exp Med*. 2003;198(5):737–746.
30. Choi JH, et al. Identification of antigen-presenting dendritic cells in mouse aorta and cardiac valves. *J Exp Med*. 2009;206(3):497–505.
31. Zhou X, Nicoletti A, Elhage R, Hansson GK. Transfer of CD4(+) T cells aggravates atherosclerosis in immunodeficient apolipoprotein E knockout mice. *Circulation*. 2000;102(24):2919–2922.
32. Zernecke A, Shagdarsuren E, Weber C. Chemokines in atherosclerosis: an update. *Arterioscler Thromb Vasc Biol*. 2008;28(11):1897–1908.
33. D'Ambrosio D, Albanesi C, Lang R, Girolomoni G, Sinigaglia F, Laudanna C. Quantitative differences in chemokine receptor engagement generate diversity in integrin-dependent lymphocyte adhesion. *J Immunol*. 2002;169(5):2303–2312.
34. Campbell JJ, et al. The chemokine receptor CCR4 in vascular recognition by cutaneous but not intestinal memory T cells. *Nature*. 1999;400(6746):776–780.
35. Hirahara K, Liu L, Clark RA, Yamanaka K, Fuhlbrigge RC, Kupper TS. The majority of human peripheral blood CD4+CD25highFoxp3+ regulatory T cells bear functional skin-homing receptors. *J Immunol*. 2006;177(7):4488–4494.
36. Chvatchko Y, et al. A key role for CC chemokine receptor 4 in lipopolysaccharide-induced endotoxic shock. *J Exp Med*. 2000;191(10):1755–1764.
37. Huser N, et al. CCR4-deficient mice show prolonged graft survival in a chronic cardiac transplant rejection model. *Eur J Immunol*. 2005;35(1):128–138.
38. Stutte S, et al. Requirement of CCL17 for CCR7- and CXCR4-dependent migration of cutaneous dendritic cells. *Proc Natl Acad Sci U S A*. 2010; 107(19):8736–8741.
39. Welte T, et al. STAT5 interaction with the T cell receptor complex and stimulation of T cell proliferation. *Science*. 1999;283(5399):222–225.
40. Nakajima H, et al. An indirect effect of Stat5a in IL-2-induced proliferation: a critical role for Stat5a in IL-2-mediated IL-2 receptor alpha chain induction. *Immunity*. 1997;7(5):691–701.
41. Vogtenhuber C, et al. Constitutively active Stat5b in CD4+ T-cells inhibits graft-versus-host disease (GVHD) lethality associated with increased regulatory T-cell (Treg) potency and decreased T effector cell (Teff) responses. *Blood*. 2010;116(3):466–474
42. Lee IH, Li WP, Hisert KB, Ivashkiv LB. Inhibition of interleukin 2 signaling and signal transducer and activator of transcription (STAT)5 activation during T cell receptor-mediated feedback inhibition of T cell expansion. *J Exp Med*. 1999;190(9):1263–1274.
43. Villarino AV, et al. Helper T cell IL-2 production is limited by negative feedback and STAT-dependent cytokine signals. *J Exp Med*. 2007;204(1):65–71.
44. Yu A, Zhu L, Altman NH, Malek TR. A low interleukin-2 receptor signaling threshold supports the development and homeostasis of T regulatory cells.

Immunity. 2009;30(2):204–217.
45. Malek TR, Castro I. Interleukin-2 receptor signaling: at the interface between tolerance and immunity. *Immunity*. 2010;33(2):153–165.
46. Yao Z, et al. Stat5a/b are essential for normal lymphoid development and differentiation. *Proc Natl Acad Sci U S A*. 2006;103(4):1000–1005.
47. Zorn E, et al. IL-2 regulates FOXP3 expression in human CD4+CD25+ regulatory T cells through a STAT-dependent mechanism and induces the expansion of these cells in vivo. *Blood*. 2006; 108(5):1571–1579.
48. Ivashkiv LB, Hu X. Signaling by STATs. *Arthritis Res Ther*. 2004;6(4):159–168.
49. Krasilnikov M, Ivanov VN, Dong J, Ronai Z. ERK and PI3K negatively regulate STAT-transcriptional activities in human melanoma cells: implications towards sensitization to apoptosis. *Oncogene*. 2003; 22(26):4092–4101.
50. Heijink IH, Vellenga E, Oostendorp J, de Monchy JG, Postma DS, Kauffman HF. Exposure to TARC alters beta2-adrenergic receptor signaling in human peripheral blood T lymphocytes. *Am J Physiol Lung Cell Mol Physiol*. 2005;289(1):L53–L59.
51. Cronshaw DG, Owen C, Brown Z, Ward SG. Activation of phosphoinositide 3-kinases by the CCR4 ligand macrophage-derived chemokine is a dispensable signal for T lymphocyte chemotaxis. *J Immunol*. 2004;172(12):7761–7770.
52. Sakaguchi S, Yamaguchi T, Nomura T, Ono M. Regulatory T cells and immune tolerance. *Cell*. 2008; 133(5):775–787.
53. Denning TL, Wang YC, Patel SR, Williams IR, Pulendran B. Lamina propria macrophages and dendritic cells differentially induce regulatory and interleukin 17-producing T cell responses. *Nat Immunol*. 2007;8(10):1086–1094.
54. Landsman L, et al. CX3CR1 is required for monocyte homeostasis and atherogenesis by promoting cell survival. *Blood*. 2009;113(4):963–972.
55. Paulsson G, Zhou X, Tornquist E, Hansson GK. Oligoclonal T cell expansions in atherosclerotic lesions of apolipoprotein E-deficient mice. *Arterioscler Thromb Vasc Biol*. 2000;20(1):10–17.
56. Tiemessen MM, Jagger AL, Evans HG, van Herwijnen MJ, John S, Taams LS. CD4+CD25+Foxp3+ regulatory T cells induce alternative activation of human monocytes/macrophages. *Proc Natl Acad Sci U S A*. 2007;104(49):19446–19451.
57. Mosser DM, Edwards JP. Exploring the full spectrum of macrophage activation. *Nat Rev Immunol*. 2008;8(12):958–969.
58. Savage ND, et al. Human anti-inflammatory macrophages induce Foxp3+ GITR+ CD25+ regulatory T cells, which suppress via membrane-bound TGF-beta-1. *J Immunol*. 2008;181(3):2220–2226.
59. Randolph GJ. Emigration of monocyte-derived cells to lymph nodes during resolution of inflammation and its failure in atherosclerosis. *Curr Opin Lipidol*. 2008;19(5):462–468.
60. Angeli V, et al. Dyslipidemia associated with atherosclerotic disease systemically alters dendritic cell mobilization. *Immunity*. 2004;21(4):561–574.
61. Luchtefeld M, et al. Chemokine receptor 7 knockout attenuates atherosclerotic plaque development. *Circulation*. 2010;122(16):1621–1628.
62. Rader DJ, Daugherty A. Translating molecular discoveries into new therapies for atherosclerosis. *Nature*. 2008;451(7181):904–913.
63. Lindquist RL, et al. Visualizing dendritic cell networks in vivo. *Nat Immunol*. 2004;5(12):1243–1250.
64. Bettelli E, et al. Reciprocal developmental pathways for the generation of pathogenic effector TH17 and regulatory T cells. *Nature*. 2006;441(7090):235–238.
65. Bernhagen J, et al. MIF is a noncognate ligand of CXC chemokine receptors in inflammatory and atherogenic cell recruitment. *Nat Med*. 2007; 13(5):587–596.
66. Megens RT, et al. Two-photon microscopy of vital murine elastic and muscular arteries. Combined structural and functional imaging with subcellular resolution. *J Vasc Res*. 2007;44(2):87–98.
67. Dambrin C, Calise D, Pieraggi MT, Thiers JC, Thomsen M. Orthotopic aortic transplantation in mice: a new model of allograft arteriosclerosis. *J Heart Lung Transplant*. 1999;18(10):946–951.
68. Zernecke A, et al. Delivery of microRNA-126 by apoptotic bodies induces CXCL12-dependent vascular protection. *Sci Signal*. 2009;2(100):ra81.
69. Hieronymus T, et al. Progressive and controlled development of mouse dendritic cells from Flt3+CD11b+ progenitors in vitro. *J Immunol*. 2005; 174(5):2552–2562.
70. Soehnlein O, et al. Neutrophil secretion products pave the way for inflammatory monocytes. *Blood*. 2008; 112(4):1461–1467.